

Measurements of time-dependent CP Asymmetries in $B \rightarrow D^{*\mp} \pi^\pm$ decays using a partial reconstruction technique

I. Adachi,¹⁰ H. Aihara,⁵¹ D. Anipko,¹ K. Arinstein,¹ T. Aso,⁵⁵ V. Aulchenko,¹
 T. Aushev,^{22,16} T. Aziz,⁴⁷ S. Bahinipati,³ A. M. Bakich,⁴⁶ V. Balagura,¹⁶ Y. Ban,³⁸
 E. Barberio,²⁵ A. Bay,²² I. Bedny,¹ K. Belous,¹⁵ V. Bhardwaj,³⁷ U. Bitenc,¹⁷ S. Blyth,²⁹
 A. Bondar,¹ A. Bozek,³¹ M. Bračko,^{24,17} J. Brodzicka,^{10,31} T. E. Browder,⁹ M.-C. Chang,⁴
 P. Chang,³⁰ Y.-W. Chang,³⁰ Y. Chao,³⁰ A. Chen,²⁸ K.-F. Chen,³⁰ B. G. Cheon,⁸
 C.-C. Chiang,³⁰ R. Chistov,¹⁶ I.-S. Cho,⁵⁷ S.-K. Choi,⁷ Y. Choi,⁴⁵ Y. K. Choi,⁴⁵ S. Cole,⁴⁶
 J. Dalseno,¹⁰ M. Danilov,¹⁶ A. Das,⁴⁷ M. Dash,⁵⁶ A. Drutskoy,³ W. Dungel,¹⁴ S. Eidelman,¹
 D. Epifanov,¹ S. Esen,³ S. Fratina,¹⁷ H. Fujii,¹⁰ M. Fujikawa,²⁷ N. Gabyshev,¹
 A. Garmash,³⁹ P. Goldenzweig,³ B. Golob,^{23,17} M. Grosse Perdekamp,^{12,40} H. Guler,⁹
 H. Guo,⁴² H. Ha,¹⁹ J. Haba,¹⁰ K. Hara,²⁶ T. Hara,³⁶ Y. Hasegawa,⁴⁴ N. C. Hastings,⁵¹
 K. Hayasaka,²⁶ H. Hayashii,²⁷ M. Hazumi,¹⁰ D. Heffernan,³⁶ T. Higuchi,¹⁰ H. Hödlmoser,⁹
 T. Hokuue,²⁶ Y. Horii,⁵⁰ Y. Hoshi,⁴⁹ K. Hoshina,⁵⁴ W.-S. Hou,³⁰ Y. B. Hsiung,³⁰
 H. J. Hyun,²¹ Y. Igarashi,¹⁰ T. Iijima,²⁶ K. Ikado,²⁶ K. Inami,²⁶ A. Ishikawa,⁴¹ H. Ishino,⁵²
 R. Itoh,¹⁰ M. Iwabuchi,⁶ M. Iwasaki,⁵¹ Y. Iwasaki,¹⁰ C. Jacoby,²² N. J. Joshi,⁴⁷ M. Kaga,²⁶
 D. H. Kah,²¹ H. Kaji,²⁶ H. Kakuno,⁵¹ J. H. Kang,⁵⁷ P. Kapusta,³¹ S. U. Kataoka,²⁷
 N. Katayama,¹⁰ H. Kawai,² T. Kawasaki,³³ A. Kibayashi,¹⁰ H. Kichimi,¹⁰ H. J. Kim,²¹
 H. O. Kim,²¹ J. H. Kim,⁴⁵ S. K. Kim,⁴³ Y. I. Kim,²¹ Y. J. Kim,⁶ K. Kinoshita,³
 S. Korpar,^{24,17} Y. Kozakai,²⁶ P. Križan,^{23,17} P. Krokovny,¹⁰ R. Kumar,³⁷ E. Kurihara,²
 Y. Kuroki,³⁶ A. Kuzmin,¹ Y.-J. Kwon,⁵⁷ S.-H. Kyeong,⁵⁷ J. S. Lange,⁵ G. Leder,¹⁴
 J. Lee,⁴³ J. S. Lee,⁴⁵ M. J. Lee,⁴³ S. E. Lee,⁴³ T. Lesiak,³¹ J. Li,⁹ A. Limosani,²⁵
 S.-W. Lin,³⁰ C. Liu,⁴² Y. Liu,⁶ D. Liventsev,¹⁶ J. MacNaughton,¹⁰ F. Mandl,¹⁴
 D. Marlow,³⁹ T. Matsumura,²⁶ A. Matyja,³¹ S. McOnie,⁴⁶ T. Medvedeva,¹⁶ Y. Mikami,⁵⁰
 K. Miyabayashi,²⁷ H. Miyata,³³ Y. Miyazaki,²⁶ R. Mizuk,¹⁶ G. R. Moloney,²⁵ T. Mori,²⁶
 T. Nagamine,⁵⁰ Y. Nagasaka,¹¹ Y. Nakahama,⁵¹ I. Nakamura,¹⁰ E. Nakano,³⁵ M. Nakao,¹⁰
 H. Nakayama,⁵¹ H. Nakazawa,²⁸ Z. Natkaniec,³¹ K. Neichi,⁴⁹ S. Nishida,¹⁰ K. Nishimura,⁹
 Y. Nishio,²⁶ I. Nishizawa,⁵³ O. Nitoh,⁵⁴ S. Noguchi,²⁷ T. Nozaki,¹⁰ A. Ogawa,⁴⁰ S. Ogawa,⁴⁸
 T. Ohshima,²⁶ S. Okuno,¹⁸ S. L. Olsen,^{9,13} S. Ono,⁵² W. Ostrowicz,³¹ H. Ozaki,¹⁰
 P. Pakhlov,¹⁶ G. Pakhlova,¹⁶ H. Palka,³¹ C. W. Park,⁴⁵ H. Park,²¹ H. K. Park,²¹
 K. S. Park,⁴⁵ N. Parslow,⁴⁶ L. S. Peak,⁴⁶ M. Pernicka,¹⁴ R. Pestotnik,¹⁷ M. Peters,⁹
 L. E. Piilonen,⁵⁶ A. Poluektov,¹ J. Rorie,⁹ M. Rozanska,³¹ H. Sahoo,⁹ Y. Sakai,¹⁰
 N. Sasao,²⁰ K. Sayeed,³ T. Schietinger,²² O. Schneider,²² P. Schönmeier,⁵⁰ J. Schümann,¹⁰
 C. Schwanda,¹⁴ A. J. Schwartz,³ R. Seidl,^{12,40} A. Sekiya,²⁷ K. Senyo,²⁶ M. E. Sevier,²⁵
 L. Shang,¹³ M. Shapkin,¹⁵ V. Shebalin,¹ C. P. Shen,⁹ H. Shibuya,⁴⁸ S. Shinomiya,³⁶
 J.-G. Shiu,³⁰ B. Shwartz,¹ V. Sidorov,¹ J. B. Singh,³⁷ A. Sokolov,¹⁵ A. Somov,³ S. Stanič,³⁴
 M. Starič,¹⁷ J. Stypula,³¹ A. Sugiyama,⁴¹ K. Sumisawa,¹⁰ T. Sumiyoshi,⁵³ S. Suzuki,⁴¹
 S. Y. Suzuki,¹⁰ O. Tajima,¹⁰ F. Takasaki,¹⁰ K. Tamai,¹⁰ N. Tamura,³³ M. Tanaka,¹⁰
 N. Taniguchi,²⁰ G. N. Taylor,²⁵ Y. Teramoto,³⁵ I. Tikhomirov,¹⁶ K. Trabelsi,¹⁰
 Y. F. Tse,²⁵ T. Tsuboyama,¹⁰ Y. Uchida,⁶ S. Uehara,¹⁰ Y. Ueki,⁵³ K. Ueno,³⁰
 T. Uglov,¹⁶ Y. Unno,⁸ S. Uno,¹⁰ P. Urquijo,²⁵ Y. Ushiroda,¹⁰ Y. Usov,¹ G. Varner,⁹

K. E. Varvell,⁴⁶ K. Vervink,²² S. Villa,²² A. Vinokurova,¹ C. C. Wang,³⁰ C. H. Wang,²⁹
J. Wang,³⁸ M.-Z. Wang,³⁰ P. Wang,¹³ X. L. Wang,¹³ M. Watanabe,³³ Y. Watanabe,¹⁸
R. Wedd,²⁵ J.-T. Wei,³⁰ J. Wicht,¹⁰ L. Widhalm,¹⁴ J. Wiechczynski,³¹ E. Won,¹⁹
B. D. Yabsley,⁴⁶ A. Yamaguchi,⁵⁰ H. Yamamoto,⁵⁰ M. Yamaoka,²⁶ Y. Yamashita,³²
M. Yamauchi,¹⁰ C. Z. Yuan,¹³ Y. Yusa,⁵⁶ C. C. Zhang,¹³ L. M. Zhang,⁴² Z. P. Zhang,⁴²
V. Zhilich,¹ V. Zhulanov,¹ T. Zivko,¹⁷ A. Zupanc,¹⁷ N. Zwahlen,²² and O. Zyukova¹

(The Belle Collaboration)

¹*Budker Institute of Nuclear Physics, Novosibirsk*

²*Chiba University, Chiba*

³*University of Cincinnati, Cincinnati, Ohio 45221*

⁴*Department of Physics, Fu Jen Catholic University, Taipei*

⁵*Justus-Liebig-Universität Gießen, Gießen*

⁶*The Graduate University for Advanced Studies, Hayama*

⁷*Gyeongsang National University, Chinju*

⁸*Hanyang University, Seoul*

⁹*University of Hawaii, Honolulu, Hawaii 96822*

¹⁰*High Energy Accelerator Research Organization (KEK), Tsukuba*

¹¹*Hiroshima Institute of Technology, Hiroshima*

¹²*University of Illinois at Urbana-Champaign, Urbana, Illinois 61801*

¹³*Institute of High Energy Physics,*

Chinese Academy of Sciences, Beijing

¹⁴*Institute of High Energy Physics, Vienna*

¹⁵*Institute of High Energy Physics, Protvino*

¹⁶*Institute for Theoretical and Experimental Physics, Moscow*

¹⁷*J. Stefan Institute, Ljubljana*

¹⁸*Kanagawa University, Yokohama*

¹⁹*Korea University, Seoul*

²⁰*Kyoto University, Kyoto*

²¹*Kyungpook National University, Taegu*

²²*École Polytechnique Fédérale de Lausanne (EPFL), Lausanne*

²³*Faculty of Mathematics and Physics, University of Ljubljana, Ljubljana*

²⁴*University of Maribor, Maribor*

²⁵*University of Melbourne, School of Physics, Victoria 3010*

²⁶*Nagoya University, Nagoya*

²⁷*Nara Women's University, Nara*

²⁸*National Central University, Chung-li*

²⁹*National United University, Miao Li*

³⁰*Department of Physics, National Taiwan University, Taipei*

³¹*H. Niewodniczanski Institute of Nuclear Physics, Krakow*

³²*Nippon Dental University, Niigata*

³³*Niigata University, Niigata*

³⁴*University of Nova Gorica, Nova Gorica*

³⁵*Osaka City University, Osaka*

³⁶*Osaka University, Osaka*

³⁷*Panjab University, Chandigarh*

³⁸*Peking University, Beijing*

- ³⁹*Princeton University, Princeton, New Jersey 08544*
⁴⁰*RIKEN BNL Research Center, Upton, New York 11973*
⁴¹*Saga University, Saga*
⁴²*University of Science and Technology of China, Hefei*
⁴³*Seoul National University, Seoul*
⁴⁴*Shinshu University, Nagano*
⁴⁵*Sungkyunkwan University, Suwon*
⁴⁶*University of Sydney, Sydney, New South Wales*
⁴⁷*Tata Institute of Fundamental Research, Mumbai*
⁴⁸*Toho University, Funabashi*
⁴⁹*Tohoku Gakuin University, Tagajo*
⁵⁰*Tohoku University, Sendai*
⁵¹*Department of Physics, University of Tokyo, Tokyo*
⁵²*Tokyo Institute of Technology, Tokyo*
⁵³*Tokyo Metropolitan University, Tokyo*
⁵⁴*Tokyo University of Agriculture and Technology, Tokyo*
⁵⁵*Toyama National College of Maritime Technology, Toyama*
⁵⁶*Virginia Polytechnic Institute and State University, Blacksburg, Virginia 24061*
⁵⁷*Yonsei University, Seoul*

Abstract

We report preliminary results on time-dependent CP asymmetries in $B \rightarrow D^{*\mp}\pi^\pm$ decays. The CP asymmetry in these decays is proportional to $2R_{D^*\pi} \sin(2\phi_1 + \phi_3 \pm \delta_{D^*\pi})$, where $R_{D^*\pi}$ is the ratio of the magnitudes of the doubly-Cabibbo-suppressed and Cabibbo-favoured amplitudes, $\delta_{D^*\pi}$ is the strong phase difference between them, and ϕ_1 and ϕ_3 are two angles of the CKM Unitarity Triangle. This study is based on a large data sample that contains 657 million $B\bar{B}$ pairs collected with the Belle detector at the KEKB asymmetric-energy e^+e^- collider at the $\Upsilon(4S)$ resonance. We use a partial reconstruction technique, wherein signal $B \rightarrow D^{*\mp}\pi^\pm$ events are identified using information only from the π^\pm from the B decay and the charged slow pion from the subsequent decay of the D^{*-} . We obtain $S^+(D^*\pi) = +0.057 \pm 0.019(\text{stat}) \pm 0.012(\text{sys})$ and $S^-(D^*\pi) = +0.038 \pm 0.020(\text{stat}) \pm 0.010(\text{sys})$.

PACS numbers:

INTRODUCTION

In the Standard Model (SM), quark flavour mixing occurs via the Cabibbo-Kobayashi-Maskawa (CKM) matrix [1]. CP violation in the SM occurs due to the presence of a complex phase in the CKM matrix. Precision measurements of the parameters of CKM matrix are of utmost importance to constrain the SM and measure the amount of CP violation. The study of the time-dependent decay rates of $B^0(\bar{B}^0) \rightarrow D^{*\mp}\pi^\pm$ provide a theoretically clean method for extracting $\sin(2\phi_1 + \phi_3)$ [2], where ϕ_1 and ϕ_3 are angles of the CKM Unitarity Triangle. As shown in Fig. 1, this decay can be mediated by both Cabibbo-favoured (CFD) and doubly-Cabibbo-suppressed (DCSD) processes, whose amplitudes are proportional to $V_{cb}^*V_{ud}$ and $V_{ub}^*V_{cd}$ respectively, which have a relative weak phase ϕ_3 .

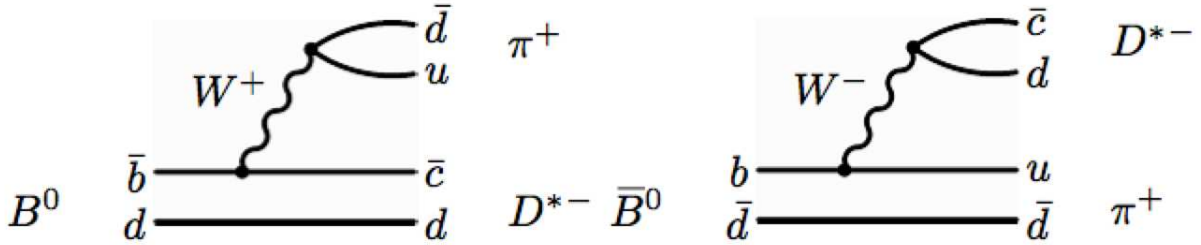


FIG. 1: Diagrams for $B^0 \rightarrow D^{*-}\pi^+$ (left) and $\bar{B}^0 \rightarrow D^{*-}\pi^+$ (right). Those for $\bar{B}^0 \rightarrow D^{*+}\pi^-$ and $B^0 \rightarrow D^{*+}\pi^-$ can be obtained by charge conjugation.

The time-dependent decay rates are given by [3]

$$\begin{aligned}
 P(B^0 \rightarrow D^{(*)\pm}\pi^\mp) &= \frac{1}{8\tau_{B^0}} e^{-|\Delta t|/\tau_{B^0}} \times [1 \mp C \cos(\Delta m \Delta t) - S^\pm \sin(\Delta m \Delta t)], \\
 P(\bar{B}^0 \rightarrow D^{(*)\pm}\pi^\mp) &= \frac{1}{8\tau_{B^0}} e^{-|\Delta t|/\tau_{B^0}} \times [1 \pm C \cos(\Delta m \Delta t) + S^\pm \sin(\Delta m \Delta t)]. \quad (1)
 \end{aligned}$$

Here Δt is the difference between the time of the decay and the time that the flavour of the B meson is tagged, τ_{B^0} is the average neutral B meson lifetime, Δm is the B^0 - \bar{B}^0 mixing parameter, and $C = (1 - R^2)/(1 + R^2)$, where R is the ratio of the magnitudes between the DCSD and CFD (we assume the magnitudes of both the CFD and DCSD amplitudes are the same for B^0 and \bar{B}^0 decays). The CP violation parameters are given by

$$S^\pm = \frac{2(-1)^L R \sin(2\phi_1 + \phi_3 \pm \delta)}{(1 + R^2)}, \quad (2)$$

where L is the orbital angular momentum of the final state (1 for $D^*\pi$), and δ is the strong phase difference between CFD and DCSD. Since the predicted value of R is small, ~ 0.02 [4], we neglect terms of $\mathcal{O}(R^2)$ (and hence take $C = 1$). The strong phase δ for $D^*\pi$ is predicted to be small [3, 5]. Since R is expected to be suppressed, the amount of CP violation in $D^*\pi$ decays, which is proportional to R , is expected to be small and a large data sample is needed in order to obtain sufficient sensitivity. We employ a partial reconstruction technique [6] for the $D^*\pi$ analysis, wherein the signal is distinguished from background on the basis of kinematics of the ‘fast’ pion (π_f) from the decay $B \rightarrow D^*\pi_f$, and the ‘slow’ pion (π_s) from the subsequent decay of $D^* \rightarrow D\pi_s$; the D meson is not reconstructed at all.

Previous analyses have been reported by Belle [7, 8] as well as by Babar [9]. This study uses a data sample of 605 fb^{-1} containing 657 million $B\bar{B}$ events, which is about two times the size of the dataset used in the previous Belle analysis [8] and supersedes the previous Belle result.

BELLE DETECTOR

The data were collected with the Belle detector [10] at the KEKB asymmetric energy electron-positron (e^-e^+) collider [11] operating at the $\Upsilon(4S)$ resonance. The Belle detector is a large-solid-angle magnetic spectrometer that consists of a silicon vertex detector (SVD), a 50-layer central drift chamber (CDC), an array of aerogel threshold Cherenkov counters (ACC), a barrel-like arrangement of time-of-flight scintillation counters (TOF), and an electromagnetic calorimeter (ECL) comprised of CsI(Tl) crystals located inside a superconducting solenoidal coil that provides a 1.5 T magnetic field. An iron flux-return located outside of the coil is instrumented to detect K_L^0 mesons and to identify muons (KLM). A sample containing 152 million $B\bar{B}$ pairs was collected with a 2.0 cm radius beam pipe and a 3-layer silicon vertex detector (SVD1), while a sample of 505 million $B\bar{B}$ pairs was collected with a 1.5 cm radius beam pipe, a 4-layer silicon vertex detector (SVD2), and a small-cell inner drift chamber [12].

ANALYSIS PROCEDURE

Partial Reconstruction of $B \rightarrow D^{*\mp}\pi^\pm$ decays

To reconstruct the CP -side tags, we use: $\bar{B} \rightarrow D^{*\pm}\pi^\mp$; $D^{*\pm} \rightarrow D^0\pi^\pm$. Candidate events are selected by requiring the presence of oppositely charged ‘ f ’ and ‘ s ’ candidates. We estimate the D^* frame using energy-momentum conservation:

$$\begin{aligned} E_{D^*} &= E_{\bar{B}^0} - E_f, \\ \vec{p}_f + \vec{p}_{D^*} &= \vec{p}_B. \end{aligned} \quad (3)$$

Here, E and p stand for energy and momentum respectively. $E_{\bar{B}^0}$ is half the total centre-of-mass energy (E_{CM}) of the incoming e^+e^- beams and $p_B = \sqrt{E_{CM}^2/4 - m_{B^0}^2}$, where m_{B^0} is the nominal B^0 mass [14]. Using E_{D^*} , the momentum of D^* can be obtained in the e^+e^- centre-of-mass (cms) as: $p_{D^*} = \sqrt{E_{D^*}^2 - m_{D^*}^2}$. We construct a partially reconstructed D^{*+} frame, using p_{D^*} and E_{D^*} and taking the direction of \vec{p}_{D^*} opposite to \vec{p}_f .

We define a variable, p_δ , which is strongly correlated with the fast pion momentum, p_f . p_δ is defined as: $||p_f| - |p_{D^*}||$ and from Eq. (3), it follows: $|p_\delta| \leq |\vec{p}_B|$ ($\approx 0.3 \text{ GeV}/c$). We boost the charged slow pion into the partially reconstructed D^* frame. In the true D^* frame, the slow pion is mono-energetic. However, in the partially reconstructed D^{*+} frame, the slow pion momentum will have a limited spread. We study the parallel and the transverse components of the momentum of the slow pion, π_s along the direction opposite to f , which are denoted as p_\parallel and p_\perp , respectively. In the true D^* frame, the p_\parallel variable has a distribution proportional to $\cos^2\theta^2$ for signal events, as the B decay is a pseudoscalar to pseudo-scalar vector transition.

***CP* side selection**

Fast pion (f) candidates are required to have a radial (longitudinal) impact parameter $dr < 0.1$ cm ($|dz| < 2.0$ cm) and to have associated hits in the SVD. We reject leptons and kaons based on information from the CDC, TOF and ACC from the fast pion candidate list. A requirement is made on the fast pion cms momentum, $1.93 \text{ GeV}/c < p_f < 2.50 \text{ GeV}/c$. Slow pion (s) candidates are required to have cms momentum in the range $0.05 \text{ GeV}/c < p_s < 0.30 \text{ GeV}/c$. Since slow pions are not used for vertexing, no particle identification requirement is applied, we impose only a loose requirement that they originate from the IP. We select candidates that satisfy $+0.00 \text{ GeV}/c < p_{\perp} < +0.06 \text{ GeV}/c$, $-0.10 \text{ GeV}/c < p_{\parallel} < 0.07 \text{ GeV}/c$ and $-0.60 \text{ GeV}/c < p_{\delta} < 0.50 \text{ GeV}/c$.

Vertexing and Flavour Tagging

The determination of the flavour of the B meson opposite to the CP -side B is essential for the Δt measurement. In order to tag the flavour of the associated B meson, we require the presence of a high-momentum lepton (l) in the event. This helps reduce background from continuum $e^+e^- \rightarrow q\bar{q}$ ($q = u, d, s, c$) processes. Tagging lepton candidates are required to be positively identified either as electrons, on the basis of information from the CDC, ECL and ACC, or as muons, on the basis of information from the CDC and the KLM. They are required to have momenta in the range $1.1 \text{ GeV}/c < p_l < 2.3 \text{ GeV}/c$, and to have an angle with the fast pion candidate that satisfies $-0.75 < \cos \delta_{\pi_f l}$ in the cms. The lower bound on the momentum and the requirement on the angle also reduce, to a negligible level (0.7%), the contribution of leptons produced from semi-leptonic decays of the unreconstructed D mesons in the $B^0 \rightarrow D^{*\mp}\pi^{\pm}$ decay chain.

Identical vertexing requirements to those for fast pion candidates are made in order to obtain an accurate z_{tag} position. To further suppress the small remaining continuum background, we impose a loose requirement on the ratio of the second to zeroth Fox-Wolfram [13] moments, $R_2 < 0.6$.

At the KEKB asymmetric-energy e^+e^- (3.5 GeV on 8 GeV) collider, operating at the $\Upsilon(4S)$ resonance ($\sqrt{s} = 10.58$ GeV), the $\Upsilon(4S)$ is produced with a Lorentz boost of $\beta\gamma = 0.425$, almost along the electron beamline (z) at KEKB. In the cms, B^0 and \bar{B}^0 mesons are approximately at rest. Hence the proper time-difference (Δt) between the z_{CP} and z_{tag} vertices is obtained from fast pion on the CP -side and the tagging lepton. The variable Δt is defined as:

$$\Delta t \approx (z_{CP} - z_{\text{tag}})/\beta\gamma c. \quad (4)$$

The CP -side (z_{CP}) vertex is obtained from the fast pion on the CP -side and the run-dependent interaction point profile (IP). The tag-side (z_{tag}) vertex is obtained from tagging lepton and the run-dependent IP.

Yield Fit

We use the three kinematic variables, p_{δ} , p_{\parallel} and p_{\perp} to distinguish between signal and background on the CP side. Background events are separated into three categories: $D^{*\mp}\rho^{\pm}$, which is kinematically similar to the signal; correlated background, in which the slow pion

originates from the decay of a D^* that originates from the decay of the same B as the fast pion candidate (*e.g.*, $D^{**}\pi$); and uncorrelated background, which includes everything else (*e.g.*, continuum processes, $D\pi$). The kinematic distributions of the signal and background categories are determined from a large MC sample, corresponding to three times the integrated luminosity of our data sample.

We select candidates that satisfy $-0.10 \text{ GeV}/c < p_{\parallel} < +0.07 \text{ GeV}/c$ and $-0.60 \text{ GeV}/c < p_{\delta} < +0.50 \text{ GeV}/c$. In the cases where more than one candidate satisfies these criteria, we select the one with the largest value of $\delta_{\pi_f\pi_s}$, where $\delta_{\pi_f\pi_s}$ is the angle between the fast pion direction and the slow pion direction in the cms frame. The signal region is defined as: $-0.40 \text{ GeV}/c < p_{\delta} < +0.40 \text{ GeV}/c$ and two regions in p_{\parallel} : $-0.05 \text{ GeV}/c < p_{\parallel} < -0.01 \text{ GeV}/c$ and $+0.01 \text{ GeV}/c < p_{\parallel} < +0.04 \text{ GeV}/c$.

Event-by-event signal and background fractions are determined from binned maximum likelihood fits to the two-dimensional kinematic distributions (p_{δ} and p_{\parallel}). The results of these fits, projected onto each of the two variables, are shown in Fig. 2, and summarized in Table I. We obtain a signal purity of $59.0 \pm 0.4\%$, where purity is defined as ratio of the signal and total yield.

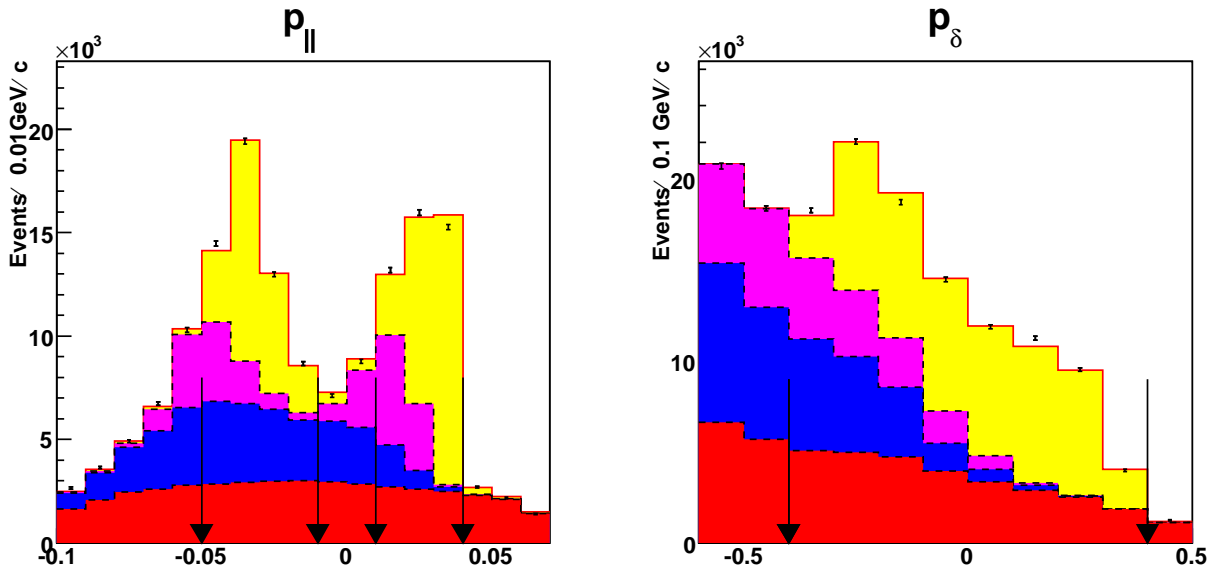


FIG. 2: Results of the yield fits to $D^*\pi$ candidates projected onto the p_{\parallel} (left) and p_{δ} (right) axes in the signal region of the kinematic variables. The contributions are: $D^*\pi$ (yellow), $D^*\rho$ (magenta), correlated background (blue) and uncorrelated background (red).

Fit Procedure to obtain CP violation parameters

We perform a simultaneous unbinned fit to the same-flavour (SF) events, in which the fast pion and the tagging lepton have the same charge, and opposite-flavour (OF) events, in which the fast pion (f) and the tagging lepton (l) have the opposite charge, to measure the CP violation parameters in the $D^*\pi$ sample. We minimize the quantity $-2 \ln \mathcal{L} = -2 \sum_i \ln \mathcal{L}_i$, where

$$\mathcal{L}_i = f_{D^*\pi} P_{D^*\pi} + f_{D^*\rho} P_{D^*\rho} + f_{\text{unco}} P_{\text{unco}} + f_{\text{corr}} P_{\text{corr}}. \quad (5)$$

TABLE I: Summary of the yields in the signal region

	Candidates
$D^*\pi$	50196 ± 286
$D^*\rho$	10232 ± 150
Correlated background	10425 ± 135
Uncorrelated background	14193 ± 128

Here, f stands for the event-by-event signal and background fractions and are obtained from the fits to the kinematic variables and P stands for the probability density functions (PDF) for signal and backgrounds, which contain a physics PDF and experimental effects. For $D^*\pi$ and $D^*\rho$, the PDF is given by Eq. (1), where for $D^*\rho$ the terms S^\pm are effective parameters averaged over the helicity states [15] and are constrained to be zero. The PDF for correlated background contains a term for neutral B decays (given by Eq. (1) with $S^\pm = 0$), and a term for charged B decays (for which the PDF is $\frac{1}{2\tau_{B^+}}e^{-|\Delta t|/\tau_{B^+}}$, where τ_{B^+} is the lifetime of the charged B meson). The PDF for uncorrelated background also contains neutral and charged B components, with the remainder from continuum $e^+e^- \rightarrow q\bar{q}$ ($q = u, d, s, c$) processes. The continuum PDF is modelled with two components: one with negligible lifetime, and the other with a finite lifetime.

The parameters in P_{unco} and P_{corr} are obtained from separate simultaneous fits to OF and SF candidates in the respective sideband regions. In these fits, the CP violation parameters are fixed to 0 since there is no CP in background. The fit is further simplified by fixing the biases in Δz to zero (discussed later in detail). Monte-Carlo simulation studies demonstrate that floating or fixing these biases to 0 does not affect the background parameters.

To measure the uncorrelated background shape, we use events in a sideband region, $-0.10 \text{ GeV}/c < p_{\parallel} < 0.07 \text{ GeV}/c$, $0.01 \text{ GeV}/c < p_{\parallel} < 0.04 \text{ GeV}/c$, $-0.60 \text{ GeV}/c < p_{\delta} < 0.50 \text{ GeV}/c$ and $0.08 \text{ GeV}/c < p_{\perp} < 0.10 \text{ GeV}/c$, which is populated mostly by uncorrelated background. To determine the correlated background parameters, we use events in a sideband region, $-0.10 \text{ GeV}/c < p_{\parallel} < 0.07 \text{ GeV}/c$, $-0.60 \text{ GeV}/c < p_{\delta} < 0.00 \text{ GeV}/c$ and $0.00 \text{ GeV}/c < p_{\perp} < 0.05 \text{ GeV}/c$. This sideband region is dominated by correlated and uncorrelated backgrounds and has very small amount of $D^*\pi$ signal and $D^*\rho$ background. The uncorrelated background parameters are fixed to the values obtained in the previous fit.

The PDF for the signal and background in Eq. (5) must be convolved with corresponding Δz resolution functions related to kinematic smearing (\mathcal{R}_k), detector resolution (\mathcal{R}_{det}), and asymmetry in Δz due to non-primary tracks (\mathcal{R}_{np}). The resolution function related to kinematic smearing is due to the fact that we use the approximation of Eq. (4). The detector resolution function parameters are obtained using $J/\psi \rightarrow \mu^+\mu^-$ candidates. Since both the fast pion and the tagging lepton originate directly from B meson decays for correctly tagged signal events, we do not include any additional smearing due to non-primary tracks in such events. However, for incorrectly tagged events, almost exclusively originating from secondary leptons or pions, the PDF is convolved with an additional resolution component whose parameters are determined from MC simulations. The detector resolution and smearing due to asymmetry in Δz due to non-primary tracks are described in detail elsewhere [8].

Mistagging is taken into account using

$$P(l_{\text{tag}}^{\mp}, \pi_f^{\pm}) = (1 - w_{\mp})P(B^0/\overline{B}^0 \rightarrow D^{*\mp}\pi^{\pm}) + w_{\pm}P(\overline{B}^0/B^0 \rightarrow D^{*\mp}\pi^{\pm}) \quad (6)$$

where π_f is fast pion in CP -side, l is tag-side lepton, w^+ and w^- are the wrong-tag fractions, defined as the probabilities to incorrectly measure the flavour of tagging B^0 and \overline{B}^0 mesons respectively and are determined from the data as free parameters in the fit for S^{\pm} .

The time difference Δt is related to the measured quantity Δz as described in Eq. (4), with an additional term due to possible offsets in the mean value of Δz ,

$$\Delta t \longrightarrow \Delta t + \epsilon_{\Delta t} \simeq (\Delta z + \epsilon_{\Delta z})/\beta\gamma c. \quad (7)$$

It is essential to allow non-zero values of $\epsilon_{\Delta t}$ since a small bias can mimic the effect of CP violation:

$$\cos(\Delta m \Delta t) \rightarrow \cos(\Delta m \Delta t) - \Delta m \epsilon_{\Delta t} \sin(\Delta m \Delta t) \quad (8)$$

A bias as small as $\epsilon_{\Delta z} \sim 1 \mu\text{m}$ can lead to sine-like terms as large as 0.01, comparable to the expected size of the CP violation effect. Because both vertex positions are obtained from single tracks, the partial reconstruction analysis is more susceptible than other Belle CP analyses to such biases. We allow separate offsets for each combination of h and l charges. In order to correct for a known bias due to the relative misalignment of the SVD and CDC in SVD1 data, a small correction is applied to each measured vertex position. This correction is dependent on the track charge, momentum and polar angle, measured in the laboratory frame and is obtained by comparing the vertex positions calculated with the alignment constants used in the data, to those obtained with an improved set of alignment constants [16], which removes the observed bias. Since the alignment in SVD2 data was found to be comparable to that of the corrected SVD1 data, no additional correction was applied to SVD2 data.

Fit Result

In order to test our fit procedure, we first constrain S^+ and S^- to be zero and perform a fit in which τ_{B^0} and Δm (as well as two wrong tag fractions and eight offsets) are free parameters. We obtain $\tau_{B^0} = 1.538 \pm 0.008 \text{ ps}$ and $\Delta m = 0.482 \pm 0.004 \text{ ps}^{-1}$, where the errors are statistical only. These values are compatible with their world average values [14]. Reasonable agreement with the input values is also obtained in MC. Furthermore, fits to the MC with S^{\pm} floated give results consistent with zero, as expected.

To extract the CP violation parameters we fix τ_{B^0} and Δm at their world average values, and fit with S^+ , S^- , two wrong tag fractions, and eight offsets as free parameters. We obtain $S^+ = 0.057 \pm 0.019$ and $S^- = 0.038 \pm 0.020$ where the errors are statistical only. The wrong tag fractions are $w_- = (6.8 \pm 0.3)\%$ and $w_+ = (6.6 \pm 0.3)\%$. All floating offsets are consistent with zero except for one of the OF combinations ($h = \pi^-$, $l = \ell^+$) in the SVD1 sample. The results are shown in Fig. 3. To further illustrate the CP violation effect, we define asymmetries in the same flavour events (\mathcal{A}^{SF}) and in the opposite flavour events (\mathcal{A}^{OF}), as

$$\begin{aligned} \mathcal{A}^{\text{SF}} &= \frac{N_{\pi^-l^-}(\Delta z) - N_{\pi^+l^+}(\Delta z)}{N_{\pi^-l^-}(\Delta z) + N_{\pi^+l^+}(\Delta z)}, \\ \mathcal{A}^{\text{OF}} &= \frac{N_{\pi^+l^-}(\Delta z) - N_{\pi^-l^+}(\Delta z)}{N_{\pi^+l^-}(\Delta z) + N_{\pi^-l^+}(\Delta z)}, \end{aligned} \quad (9)$$

where the N values indicate the number of events for each combination of h and l charge. These are shown in Fig. 4.

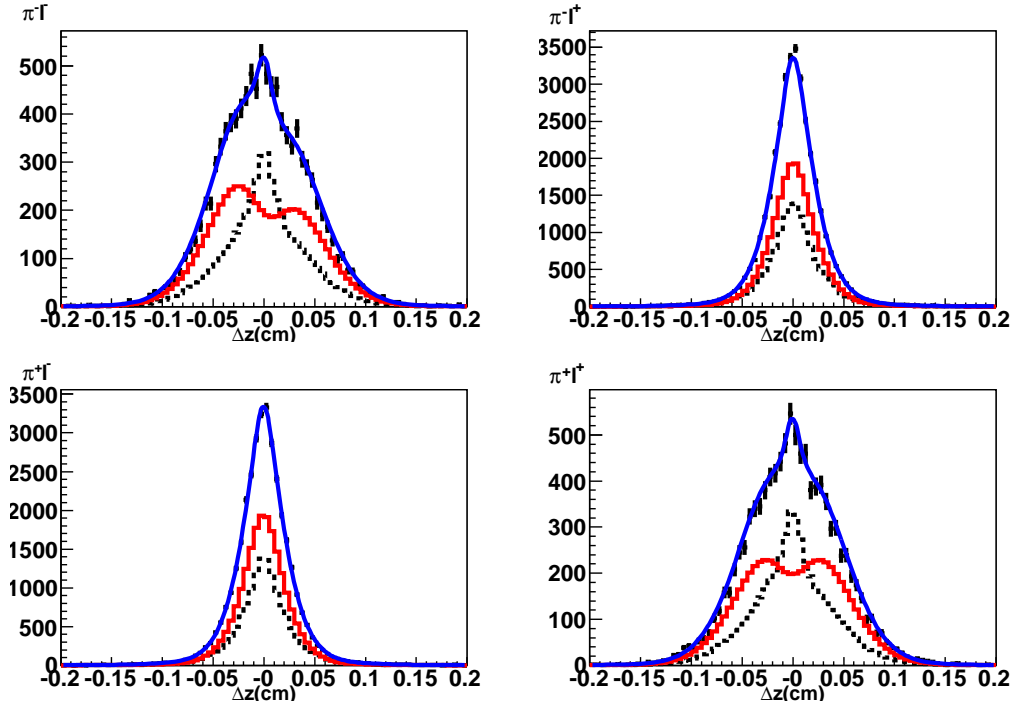


FIG. 3: Δz distributions for 4 flavour-charge combinations: $\pi^- l^-$ (top left), $\pi^- l^+$ (top right), $\pi^+ l^-$ (bottom left), $\pi^+ l^+$ (bottom right). The fit result is superimposed on the data (blue line). The signal and background components are shown as the red and dotted black curves, respectively.

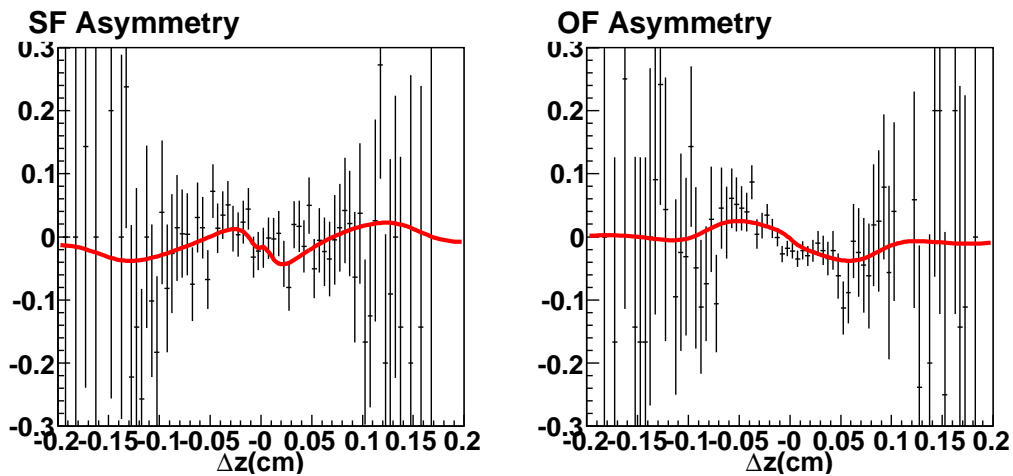


FIG. 4: Results of the fit to obtain S^+ and S^- , shown as asymmetries in the same flavour events (left) and opposite flavour events (right). The fit result (red curve) is superimposed on the data.

Systematic Error

This analysis is very sensitive to the vertexing bias. Hence, we have use Δz offsets in the fits to take care of this bias. In order to estimate the error due to these offsets, we use the difference of the mean of S^\pm obtained using an ensemble of 300 generated $D^*\pi$ signal samples with CP ($S^\pm = -0.04$) and the generated CP value.

Other sources of systematic error are the parameters of resolution functions, \mathcal{R}_k , \mathcal{R}_{det} and \mathcal{R}_{np} , the parameters of uncorrelated and correlated background and physics parameters, Δm , τ_{B^0} , τ_{B^+} , $S_{D^*\rho}^\pm$ and S_{corr}^\pm that are fixed in the CP fit, where S_{corr}^\pm are the CP violation parameters for the correlated background component ($S_{corr}^\pm = \pm 0.05$ in the CP fit). Additional systematic errors can result from varying the number of bins for the kinematic variables, p_δ and p_\parallel in the yield fit.

We use a triple Gaussian as the detector resolution (R_{det}) function model. We consider the systematic uncertainty due to lack of knowledge of the exact functional form of the resolution model. Hence, we change the resolution models and obtain shifts as large as 0.008 for S^+ . This is conservatively assigned as the systematic error due to lack of knowledge of the resolution model.

We also performed a linearity test to check for possible fit bias by generating a number of large samples of signal MC simulations with different input values of S^+ and S^- . All results are consistent with the input values, without evidence of any bias. In addition, we checked the pull for S^+ and S^- using two types of ensembles, one set generated with no CP ($S^\pm = 0$) and the other with CP ($S^\pm = -0.04$) and obtained mean (m) and rms (σ) of the pull distributions fitted to a single Gaussian. For the no CP case, $m_{S^+} = +0.10 \pm 0.06$, $\sigma_{S^+} = +0.94 \pm 0.05$; $m_{S^-} = -0.10 \pm 0.06$, $\sigma_{S^-} = +0.96 \pm 0.05$ and for the case with CP , $m_{S^+} = +0.14 \pm 0.07$, $\sigma_{S^+} = +1.10 \pm 0.06$; $m_{S^-} = -0.29 \pm 0.06$, $\sigma_{S^-} = +0.98 \pm 0.05$. Both cases yield m and σ for the pull distributions close to 0 and 1, respectively. This shows that our fit routine does not have any significant bias.

The systematic errors are summarized in Table II. The total systematic error is obtained by adding the above terms in quadrature.

Systematic error source	S^+	S^-
Δz offset	0.002	0.003
\mathcal{R}_k parameters	0.002	0.003
\mathcal{R}_{det} parameters	0.002	0.002
\mathcal{R}_{np} parameters	0.008	0.007
Background parameters	0.002	0.003
Physics parameters	0.004	0.004
Yield fit	0.003	0.003
Resolution model	0.006	0.002
Δz floated in background PDF	0.000	0.000
Total systematic error	0.012	0.010

TABLE II: Summary of possible sources of systematic error

The results using the partial reconstruction method are

$$\begin{aligned} S^+ &= +0.057 \pm 0.019 \pm 0.012, \\ S^- &= +0.038 \pm 0.020 \pm 0.010, \end{aligned} \tag{10}$$

where the first error is statistical and the second error is systematic.

SUMMARY

We have measured CP violation parameters that depend on ϕ_3 using the time-dependent decay rates of the decay $B^0 \rightarrow D^{*\mp}\pi^\pm$ using a data sample containing 657 million $B\bar{B}$ events. We obtain the CP violation parameters expressed in terms of S^+ and S^- , which are related to the CKM angles ϕ_1 and ϕ_3 , the ratio of suppressed to favoured amplitudes, and the strong phase difference between them, as $S^\pm = -R_{D^*\pi} \sin(2\phi_1 + \phi_3 \pm \delta_{D^*\pi}) / (1 + R_{D^*\pi}^2)$ for $D^*\pi$ as

$$\begin{aligned} S^+ &= +0.057 \pm 0.019 \pm 0.012, \\ S^- &= +0.038 \pm 0.020 \pm 0.010, \end{aligned} \tag{11}$$

where the first errors are statistical and the second errors are systematic.

Acknowledgements

We thank the KEKB group for the excellent operation of the accelerator, the KEK cryogenics group for the efficient operation of the solenoid, and the KEK computer group and the National Institute of Informatics for valuable computing and SINET3 network support. We acknowledge support from the Ministry of Education, Culture, Sports, Science, and Technology of Japan and the Japan Society for the Promotion of Science; the Australian Research Council and the Australian Department of Education, Science and Training; the National Natural Science Foundation of China under contract No. 10575109 and 10775142; the Department of Science and Technology of India; the BK21 program of the Ministry of Education of Korea, the CHEP src program and Basic Research program (grant No. R01-2005-000-10089-0, R01-2008-000-10477-0) of the Korea Science and Engineering Foundation; the Polish State Committee for Scientific Research; the Ministry of Education and Science of the Russian Federation and the Russian Federal Agency for Atomic Energy; the Slovenian Research Agency; the Swiss National Science Foundation; the National Science Council and the Ministry of Education of Taiwan; and the U.S. Department of Energy.

-
- [1] M. Kobayashi and T. Maskawa, Prog. Theor. Phys. **49** 652 (1973); N. Cabibbo, Phys. Rev. Lett. **10**, 531 (1963).
 - [2] I. Dunietz and R.G. Sachs, Phys. Rev. D **37** 3186 (1988), *Erratum*: Phys. Rev. D **39** 3515 (1989); I. Dunietz, Phys. Lett. B **427** 179 (1998).
 - [3] R. Fleischer, Nucl. Phys. B **671** 459 (2003).

- [4] D.A. Suprun, C.-W. Chiang and J.L. Rosner, Phys. Rev. D **65** 054025 (2002).
- [5] L. Wolfenstein, Phys. Rev. D **69** 016006 (2004).
- [6] Y. Zheng, T.E. Browder *et al.* (Belle Collaboration), Phys. Rev. D **67**, 092004 (2003).
- [7] T. Gershon *et al.* (Belle Collaboration), Phys. Lett. B **624**, 11 (2005).
- [8] F.J. Ronga *et al.* (Belle Collaboration), Phys. Rev. D **73** (2006) 092003
- [9] B. Aubert *et al.* (BaBar Collaboration), Phys. Rev. D **71**, 112003 (2005).
- [10] A. Abashian *et al.* (Belle Collaboration), Nucl. Instr. and Meth. A **479**, 117 (2002).
- [11] S. Kurokawa, Nucl. Instr. and Meth. A **499**,1 (2003) and other papers included in this Volume.
- [12] Z.Natkaniec *et al.* (Belle SVD2 Group), Nucl. Instrum. Methods Phys. Res. Sect. A **560**, 1(2006).
- [13] G.C. Fox and S. Wolfram, Phys. Rev. Lett. **41** 1581 (1978).
- [14] W.-M.Yao et al. (Particle Data Group), J. Phys. G 33, 1 (2006)
- [15] N. Sinha and R. Sinha, Phys. Rev. Lett. **80**, 3706 (1998), D. London, N. Sinha and R. Sinha, Phys. Rev. Lett. **85**, 1807 (2000).
- [16] A small amount of data is reprocessed using a set of constants which is corrected for the small relative misalignment of the SVD and CDC. The correction function is calculated from comparisons of the vertex positions for tracks between the two reprocessings.